NANOSTRUCTURED MATERIALS FOR SOLAR ENERGY CONVERSION

P. Oelhafen[1] and A. Schüler[2]

1: Institute of Physics University of Basel, CH-4056 Basel, Switzerland
2: LESO-EPFL, CH-1015 Lausanne, Switzerland

ABSTRACT

This paper deals with the motivation for using nanostructured materials in the field of solar energy conversion. We discuss briefly some recent fundamental observations on supported nanoclusters and optical properties of embedded metallic nanoclusters in a dielectric matrix. An overview on current research and existing applications in this field is given. Nanocomposite thin films developed for the application as optically selective absorber coatings in thermal solar collectors are described in some more detail.

INTRODUCTION

Fundamental properties of nanostructured materials are currently excessively studied because of their potential application in numerous fields such as electronic devices, opto-electronics, optics, tribology, biotechnology, human medicine and others. Since materials science is also an important issue in solar energy conversion, an increasing number of studies particularly related to materials structured on the nanometer length scale can be found in literature in the last decade. The aim of the present paper is to reveal at least for some potential applications the motivation for using nanostructured materials in solar energy conversion and to give an overview on current research topics in this field. Finally we would like to discuss in some more detail existing applications of nanostructured materials in the field of thermal energy conversion of solar radiation.

MOTIVATION FOR USING NANOSTRUCTURED MATERIALS IN SOLAR ENERGY CONVERSION

Nanostructured materials contain structures with dimensions in the nanometer length scale such as polycrystalline materials with nanometer sized crystallites (e.g. nanocrystalline silicon), materials with surface protrusions spatially separated by some nanometer (e.g. surfaces of titanium-aluminum nitride films), granular or porous materials with grain sizes in the nanometer range (e.g. titanium oxide) or nanometer sized metallic clusters embedded in a dielectric matrix (e.g. chromium carbide clusters in diamond-like carbon), to mention just a few examples.

The motivation for using nanostructured materials emerges from the specific physical and chemical properties of nanostructures. A particle containing only a few atoms (e.g. Au_3) reveals molecule-like properties. In this case the electronic states are discrete, the valence electrons cannot form a conduction band and clusters of this type cannot exhibit metallic behavior. If we increase the cluster to a few hundred atoms (e.g. a Au_{309} cluster with a diameter of about 2 nm) the particle's properties are already close to those of a bulk piece of gold, i.e. an electronic conduction band is formed and the cluster is metallic. In many cases, the interesting size range is located near the transition where properties are changing from molecular to bulk-like, a size range in which properties can be tuned in many cases in an unique way in order to design a material for a particular application.

In order to illustrate the size sensitivity of physical or chemical properties of nanometer sized clusters we are presenting some interesting features of Au nanoparticles in the next section.

Size dependent properties of gold clusters

Two examples of size dependent properties of Au nanoclusters are presented in this section. The first one is related to a metal-to-insulator transition of Au_{55} clusters with a diameter of 1.4□m. These clusters have been prepared now for more than 20 years by making use of the increased stability of the closed shell cluster structure with a 'magic number' of atoms[1]. As prepared by the wet-chemical method the cluster is covered by an organic triphenyl-phosphine ligand shell, $(PPh_3)_{12}Cl_6$. This cluster compound is ideally suited to form a two-dimensional monomolecular layer on top of a substrate with a well-defined separation between the monodisperse particles. Although this cluster compound is well known for a long time, the conductivity character of the cluster in the core of the compound was controversial until recently. The electronic structure of these aggregates has been re-examined more carefully by photoelectron spectroscopy in ultra-high-vacuum[2]. A series of valence band spectra clearly revealed the crucial role of the chlorine atoms directly bound to the Au clusters. The spectra in fig. 1a show the valence band spectra of a reference Au film along with those of naked Au clusters with a diameter of 1.6□m, the intact cluster compound (Au_{55}-L) and that of a sample after prolonged irradiation with x-rays (Au_{55}-C). Core level spectroscopy clearly showed that the chlorine atoms are desorbed after this irradiation with x-rays. The metallic character of the Au clusters can be seen from the presence of the Fermi edge (located at a binding energy of 0□eV), best visible in the spectrum of the Au reference film. A similar edge is visible in the spectra of the 1.6□m and Au_{55}-C clusters.

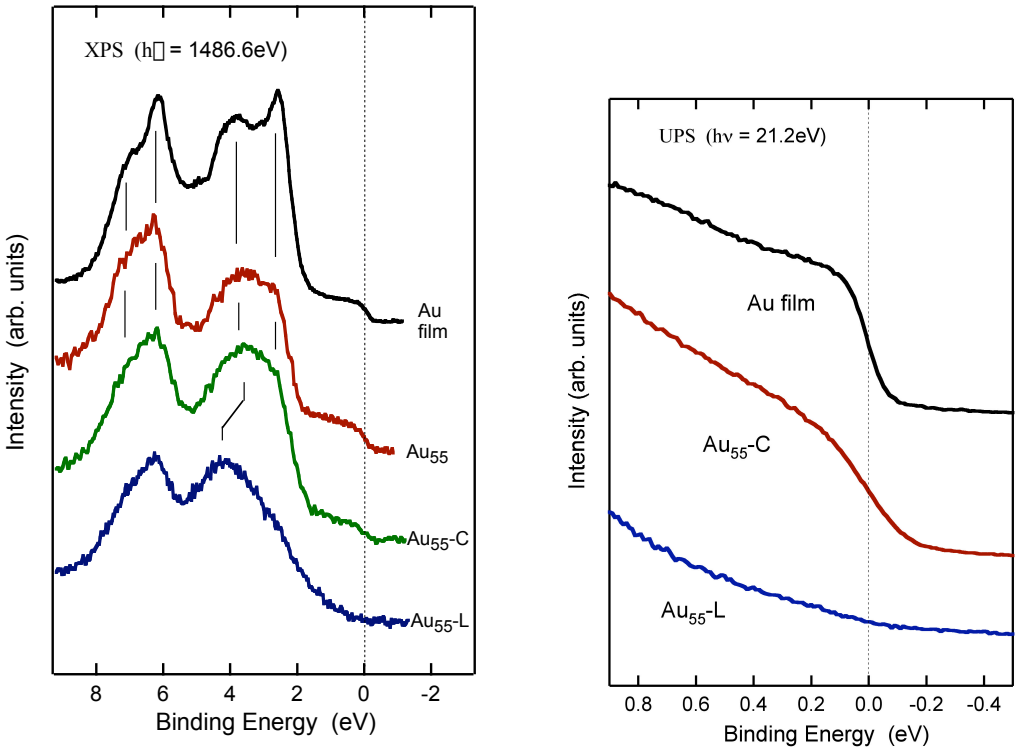

Figure 1a. (left): XPS valence band spectra of a Au reference film, naked supported Au clusters with a diameter of 1.6□m, a monomolecular layer of the intact cluster compound (Au_{55}-L) and the compound after prolonged x-ray irradiation causing the Cl desorption (Au_{55}-C). Figure 1b (right): UPS valence band spectra showing the vicinity of the Fermi energy. Note the absence of the Fermi edge in the Au_{55}-L sample.[2]

Figure 1b shows the region of the Fermi energy with a better signal-to-noise ratio measured with ultraviolet photoelectron spectroscopy. From this figure it is evident that the cluster

compound after desorption of the Cl atoms (Au_{55}-C) is metallic in contrast to the intact ligated compound (Au_{55}-L). This demonstrates that Cl desorption causes a transition from the insulating to the metallic state. The insulating state of the intact cluster compound has to be attributed to a charge transfer from the Au_{55} cluster to the 6 Cl atoms. Effects of this kind are of great interest since metal-insulator transitions are accompanied also by marked changes in the optical properties of the underlying material. Although we do not suggest a direct application of the present cluster compound, the example illustrates that nanometer sized clusters may reveal indeed unique properties.

Another interesting effect recently discovered is related to the chemical properties of naked supported Au_{55} clusters[3]. The cluster compound mentioned above has been used again in this study along with micelles containing Au clusters in the size range of about 1□m up to 8□m in the core of an organic shell. Micelles can also be deposited on top of a substrate and may form an ordered array of clusters by self-organization (see fig. 2)[3].

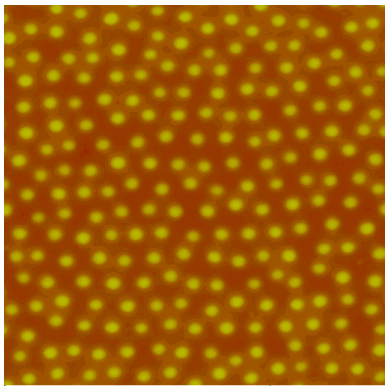

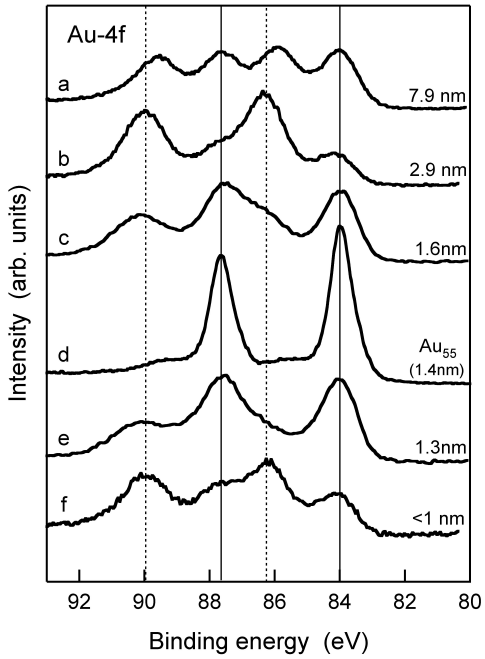

Figure 2 (left): Atomic force microscopy (AFM) image of 8□m Au clusters prepared by the micellar method (image size 1x1 micrometer, z-range 20□m)[3].

Figure 3 (right: Au 4f core level spectra of Au particles (size 1 to 8□m) obtained after exposure to reactive oxygen species provided by an in-situ rf-plasma. The vertical lines indicate the binding energy positions corresponding to elemental Au[3].

The preparation of the naked, supported Au clusters has been realized by an in-situ oxygen plasma treatment prior to the photoelectron spectroscopy measurements. The plasma treatment turned out to be an efficient tool in order to remove the ligand shells, which could be checked by XPS core level spectroscopy. In addition, the plasma treatment has been used to oxidize bulk Au and the Au clusters. A flat Au[111] surface revealed a surface Au_2O_3 layer with a thickness of 2.9□m after 10□minutes plasma exposure. The ability to form an Au oxide surface layer in the case of the Au clusters turned out to depend critically on the cluster size. Figure 3 shows the Au 4f core level spectra of supported Au clusters with different diameters. The vertical full lines at binding energies near 88 and 84□eV indicate the positions of the $Au_{5/2}$ and $Au_{7/2}$ doublet of pure metallic Au. Gold oxide reveals an Au 4f doublet shifted by some 2□eV with respect to pure Au to larger binding energies (dashed vertical lines). Hence, all clusters shown in fig. 3 except Au_{55} reveal a metallic and an oxide component with different

relative ratios depending on the diameters of the clusters. In contrast, the closed shell Au_{55} clusters could not be oxidized. This demonstrates a distinct size dependence of the chemical reactivity of these clusters, indicating again that unique phenomenon may come up when dealing with structures in the nanometer size range.

Optical properties of embedded clusters

The clusters discussed above have been studied as supported two dimensional layers on substrates. In applications related to solar energy conversion metallic clusters embedded in an insulating (dielectric) matrix are of particular interest. Existing applications in this field will be discussed below in more detail. Here we would like to focus on the special role of the nanoclusters in optical films with spectral selective absorption. We are using again Au clusters as an example now embedded in a matrix consisting of hydrogenated amorphous carbon a-C:H ('diamond-like carbon', DLC). A transmission electron microscopy (TEM) image of such a nanocomposite is shown in fig. 4.

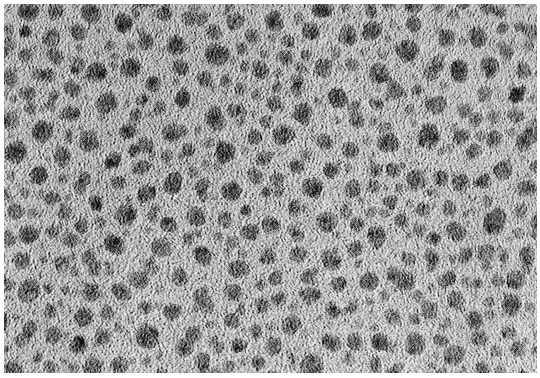

Figure 4: TEM image of an a-C:H/Au nanocomposite film. The Au particles appear as dark aggregates. The Au content of the film is 11.9□at%. The mean cluster diameter is about 2□nm.[4]

Nanocomposites of this type can easily be prepared by plasma assisted vacuum deposition processes. In the present case a plasma CVD (chemical vapor deposition) process has been combined with magnetron sputtering[4-7]. A mixture of methane and argon has been used as process gas. The former gas represents the carbon and hydrogen source for the film matrix while the energetic Ar-ions are responsible for sputtering Au atoms from an Au target to be deposited on the substrate. Due to the low solubility of Au in the carbonaceous matrix a two-phase system is formed. Figure 4 reveals important features of the cluster morphology spontaneously formed during film growth. The clusters are well separated from each other and do not tend to agglomerate. In addition, though the clusters are not monodisperse the size distribution covers a well-defined size range. The Au content of the film and the mean cluster size are correlated parameters: the cluster size decreases with decreasing Au content. As long as the clusters are spatially separated from each other the films are electrically insulating and appear purple. At a critical concentration of about 30□at% the percolation limit is reached and the films become conducting and appear golden. The optical constants n and k of some a-C:H/Au films with different Au contents are shown in fig. 5.

The optical constants of the a-C:H/Au films reveal with increasing Au content a behavior deviating more and more from that of a-C:H. The extinction coefficient exhibits a distinct absorption resonance at about 550□nm and a step in the refractive coefficient develops. It is important to note that these features are not present in the optical constants of bulk Au. The absorption resonance (also denoted as plasmon resonance) can be explained qualitatively by resonant oscillations of surface charges of the Au spheres in the field of the electromagnetic light wave. If the metallic spheres are imbedded in a dielectric matrix the interaction between the spheres and the matrix has to be taken into account by so called effective medium theories (a brief overview is given in reference[8]). In the present case (approximately spherical

particles, homogeneously distributed) the Maxwell-Garnett theory can be applied below the percolation limit. By applying several corrections such as deviations from the spherical shape of the metal clusters, an experimentally observed narrowing of the Au 5d band and taking into account the reduced mean free path of conduction electrons in the nanometer-sized clusters the concentration dependence of the effective-medium resonance (i.e. the peak near 550□m in the extinction coefficient) can be explained theoretically[9].

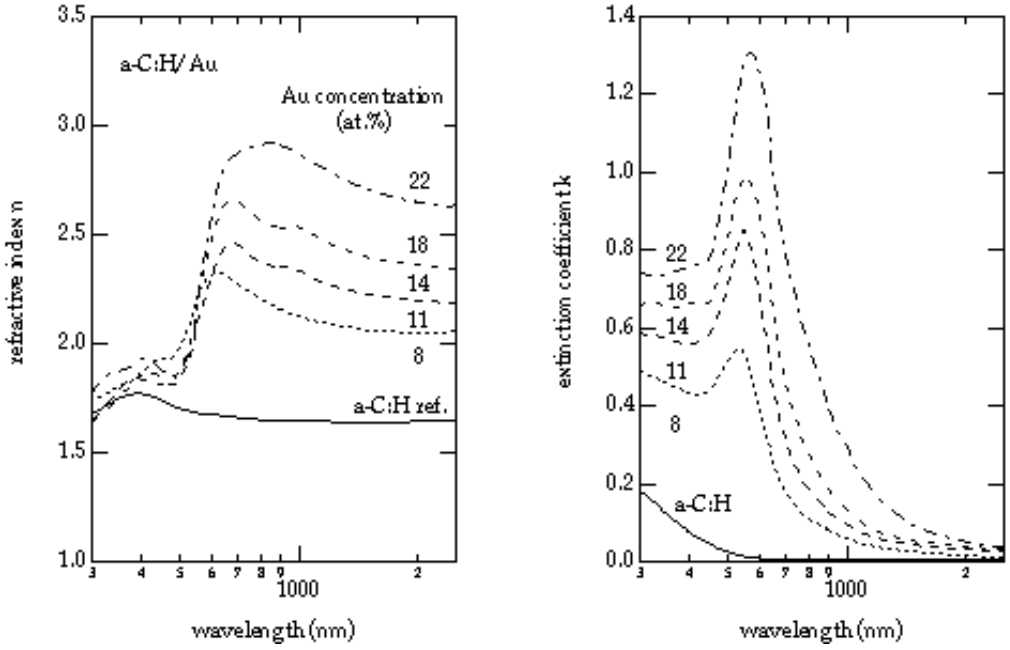

Figure 5: Refractive index n and extinction coefficient k of a-C:H/Au films with different Au concentrations (given here in at%) along with an a-C:H reference film[4].

Nanocomposites of the type discussed here play an important role as spectral selective absorber coatings in thermal solar collectors (see below). In addition, nanoparticle-doped polymer foils for use in solar control glazing that make use of absorption properties in near infrared wavelength range have been discussed recently[10]. It might amuse the reader that, without knowing the physics of the plasmon resonance of Au clusters, this effect has been exploited for several hundred years in order to color church windows by incorporation of gold particles into glass panes.

PRESENT STATE OF RESEARCH AND APPLICATION OF NANOSTRUCTURED MATERIALS IN SOLAR ENERGY CONVERSION

Table 1 gives an overview of nanostructured materials in solar energy research and application. A literature search for the topics ‘nanomaterials’ and ‘solar energy’ shows that an overwhelming part of studies in this field is related to dye-sensitized solar cells. These cells are based on a few micrometer thick layer of monodispersed TiO_2 particles in a redox electrolyte confined between two conducting glass electrodes. Light absorption is mediated by an adsorbed dye at the TiO_2 surface. In contrast to solid state photovoltaic cells photoelectrochemical cells can be manufactured relatively cheap and high conversion coefficients have recently been achieved in new devices[11]. Nanostructured oxide layers also play an important role in the field of switchable optical coatings (photoelectrochromic devices)[12, 13]. Nanocrystalline TiO_2 layers on glass have been used as a photocatalyst for solar decontamination of organic pollutants in water[14]. Nanocrystalline MgH prepared by high energy ball milling powders mixed with different transition metal oxides have been studied as a hydrogen storage material. It has been shown that the sorption kinetics could be

significantly improved by the choice of an appropriate oxide catalyst. Moreover, Mg absorbs hydrogen already at room temperature and H-release is observed as low as 200°C[15].

material	physical effect related to nanostructures	application type	realization of application
nanostructured and nanoporous metal oxides	large specific surface area, high diffusion rates	**dye-sensitized solar cells**	prototypes, pilot series
		switchable optical coatings(photoelectrochromic devices) for smart windows and translucent facades	prototypes, pilot series
	photocatalysis	**detoxification of water self-cleaning glass panes**	prototypes industrial production
	hydride formation, hydrogen storage	**hydrogen storage**	lab experiments
nanostructured and nanoporous insulators	cell size dependent thermal conductivity	**thermal insulators**	industrial production (aerogels), application prototypes
	optical properties	**low reflection coatings**	application prototypes
embedded metallic nanoclusters (nanocomposites, cermets)	optical and electronic properties of nanoclusters	**selective solar absorbers**	industrial large scale production
nanoparticle doped polymers	selective optical absorption	**solar control glazing**	lab experiments
nanostructured surfaces	perfect non-wetting (Lotus effect)	**self-cleaning surfaces**	lab experiments

Table 1: nanostructured materials for solar energy conversion and energy related applications of nanostructured materials.

Nanostructured materials such as aerogels have been investigated as thermal insulators e.g. in translucent glazings[16] or in flat plate solar collectors[17]. Silica particle films prepared by dip-coating from a sol-gel have been studied as antireflection coatings on glass and significant increase in visible transmittance could be achieved[18].

Nanocomposites consisting of nanometer-sized metal clusters embedded in a dielectric matrix (cermets) have been studied extensively and are presently applied as selective absorbers in solar collectors. Absorber coatings of this type are presently produced by vacuum based, plasma assisted deposition techniques on a large scale by several manufacturers and represents therefore *the* example for industrial application of nanostructured materials in solar energy technology. This application is discussed in more detail in the next paragraph. As already mentioned in the previous section embedded nanoparticles in relatively thick polymer foils are currently discussed as optical materials in solar control glazing[10, 19].

Another application not directly related to solar energy conversion is based on nanostructured surfaces that reveal self-cleaning behavior[20, 21]. However, such self-cleaning surfaces can even be prepared to be solar selective[22], but appeared to be mechanically not stable enough to withstand e.g. wiping with a cloth.

SELECTIVE SOLAR ABSORBERS FOR THERMAL SOLAR COLLECTORS

Optical selectivity

The power density P of thermal radiation emitted by a black body of the temperature T is described by the law of Stefan-Boltzmann:

$$P = \sigma T^4 \qquad (1)$$

with the Stefan-Boltzmann constant $\sigma = 5.67 \times 10^{-8}\ W/m^2K^4$.

According to Kirchhoff's law, the thermal emittance $\varepsilon(\lambda)$ equals always the absorptance $\alpha(\lambda)$, and for opaque surfaces both relate to the total hemispherical reflectance $R(\lambda)$:

$$\varepsilon(\lambda) = \alpha(\lambda) = 1\text{-}R(\lambda) \tag{2}$$

The solar absorptance α_{sol} is obtained by the normalized integral of the product of $\alpha(\lambda)$ and the solar spectrum AM1.5. The thermal emittance $\varepsilon_{100°C}$ is computed analogously by the integration of $\varepsilon(\lambda)$ with the spectrum of the blackbody radiation at 100°C.

Let us consider a thermal solar collector with a perfectly black absorber. A temperature of 80°C is a commonly achieved by thermal solar collectors. According to the Stefan-Boltzmann law (1), an absorber would emit under these conditions some 900 W/m^2, which is already in the order of the incident solar energy at ground level. In order to reduce these tremendous energy losses, the concept of an optically selective absorber surface is introduced. Fortunately, the spectral regions of the solar radiation and the thermal radiation emitted by the hot absorber are well separated. As shown in fig. 6 the solar radiation at ground level extends from the wavelength of 250 nm to 2500 nm, while the largest part of the thermal radiation is found in the infrared with wavelengths above 2500 nm. The ideal behavior of an absorber surface is a high absorptance in the solar spectral region and a low emittance in the range of thermal radiation, which implies a step-like reflectance spectrum with R = 0 in the solar region and R = 1 in the infrared range. A surface approaching this property is called optical selective.

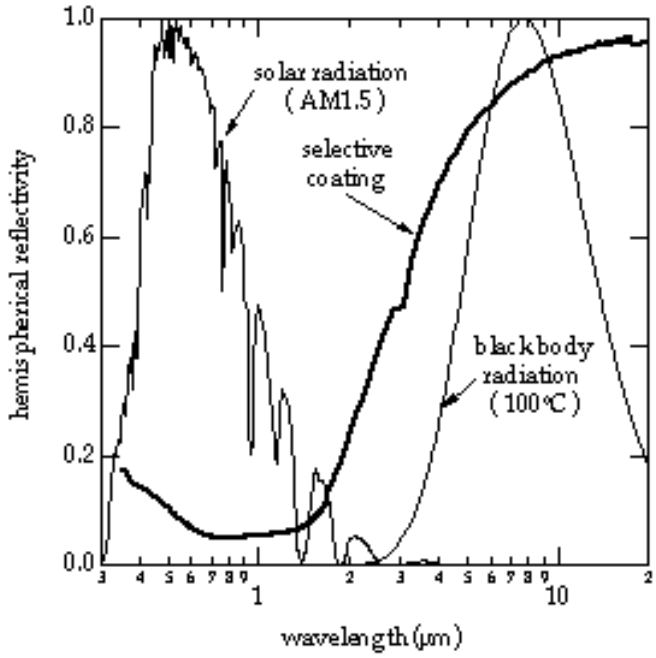

Figure 6: Solar radiation AM1.5, black body radiation at 100°C and hemispherical reflection of an optically selective a-C:H/Cr coating

In nature, no perfect intrinsically selective material has been found so far. Two ways can be followed to achieve optical selectivity: I. opposite to a black absorber a heat mirror is placed, reflecting the thermal radiation in the IR, and transmitting the solar radiation. This heat mirror can be realized by a coating on the cover glass of the collector. II. A special coating, which absorbs the solar radiation, but transmits the IR, is deposited onto a IR-reflecting substrate. Since the absorber sheet has to be treated anyways, most activities focus on the latter approach. This special coating can be a semiconductor (IR transparency due to band gap), an interference multilayer stack, a metal-dielectric (nano-)composite material with concentration gradient, or a rough coating. A comprehensive survey is given e.g. in ref. [23]. In 1955, Tabor patented an absorber coating produced by electrogalvanization[24]. Since then, the so-called

"black chrome" has become one of the standard products on the market. More recently, interest in vacuum-deposited coatings has been risen. These production processes avoid wastes (no galvanic solutions necessary), and their reproducibility makes a high quality possible. Coating materials are based on e.g. cobalt containing aluminum oxide[8], titanium oxynitride[25], chromium oxynitride[26], or metal containing amorphous hydrogenated carbon[27, 28].

Vacuum deposition and properties of individual films

Thin films are deposited inside a vacuum chamber by a combined PVD/PECVD process (PVD: physical vacuum deposition, PECVD: plasma enhanced chemical vapor deposition). Depending on the choice of target materials (e.g. Au, W, Cr, Ti, Si …) and process gases (e.g. Ar, CH4 …), a large variety of materials can be formed. We studied in detail noble and transition metal doped amorphous hydrogenated carbon a-C:H/NM (NM=Cu, Ag, Au), a-C:H/TM (TM = W, Cr, Ti), and transition metal doped amorphous hydrogenated silicon-carbon a-Si:C:H/TM (TM = Cr, Ti). In our laboratory, samples can be transferred *in situ* (without breaking the vacuum) from the deposition chamber into an electron spectrometer. X-ray and UV photoelectron spectroscopy (XPS,UPS) yield information on the chemical composition and electronic properties of the film surface. In many cases, even structural information can be inferred. Film properties depends on numerous process parameters, such as partial pressure and mass flow of process gases, power on targets, pulse frequency and shape, substrate temperature, substrate bias/plasma bias voltage, and chamber geometry. For the example of a-Si:C:H/Ti films, the dependence of elemental composition on some process parameters is visualized within the concentration triangle Si-C-Ti (fig.6). Changing one process parameter at a time results in a trajectory within this triangle[6].

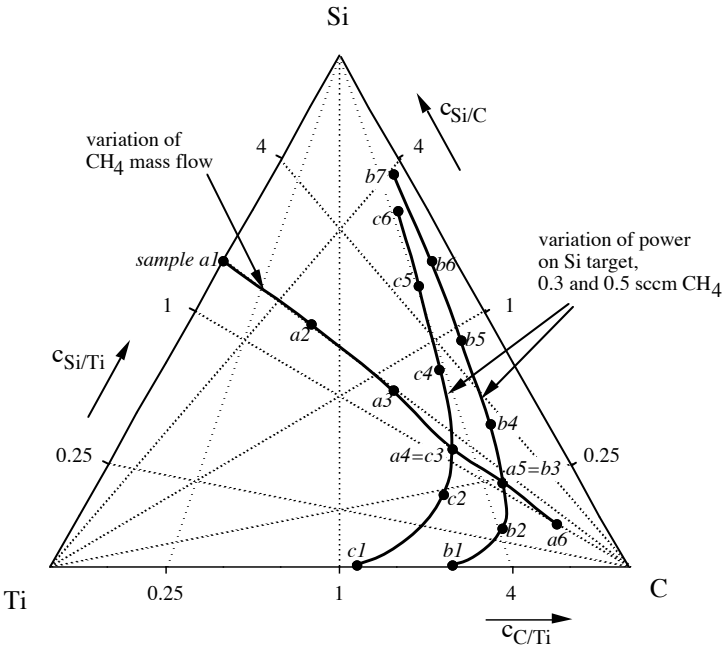

Figure 7: Compositions of a-$Si_{1-x}C_x$:H/Ti films, visualized in the concentration triangle Ti-C-Si. The solid lines indicate the dependence of the film composition on the process parameters CH_4 mass flow and power on the Si target. The labels a1,..., c6 denote different samples used in the experiment.

Chemical shifts in the XPS core lines yield evidence for the presence of metallic and dielectric film components. For transition metal containing films, the metallic component consists of carbides or ternary silicon-carbon-metal compounds. The size of the metallic aggregates can be estimated from a shift in the Fermi-edge appearing in the valence band spectra, and turns out to be in the order of several nanometers[29]. These nanostructures are

formed by self-organization during the coating process (top-down approach), and can in some cases be imaged directly by transmission electron microscopy TEM (see fig. 4).

Since the particles sizes are well below the wavelength of light, the optical properties of nanocomposite materials can be modeled within the framework of the effective medium theories, which allow to calculate the optical constants of a composite material from the optical constants of the components. Such theories have been formulated by Maxwell-Garnett[30, 31], Bruggemann[32], and Ping Sheng[33]. The differences between these theories are due the assumed geometries of the underlying models. As mentioned above, eventual non-spherical shape and the size-dependence of the optical constants for small clusters have to be taken into account.

The theoretical predictions of the optical constants have been compared to experimental measurements by spectrophotometry and real-time laser-reflectometry[9, 34]. Rather good agreement has been found. The optical constants of the nanocomposite materials can be tuned in a wide range by controlling the metal content. This feature is important for the design of graded multilayers or gradient layers.

Multilayered absorber coatings and aging tests

In order to combine the desired optical selectivity with high durability, absorber coatings are built up as a stack of multiple layers. In most cases, a good infrared mirror, such as Cu or Al, is taken as a substrate. A first layer, serving as a diffusion barrier, is applied to the substrate and subsequently covered by the functional absorber layer, which is eventually graded with respect to the metal content. A top layer repels humidity and protects the system against oxidation. Additional interlayers might be added in order to promote adhesion. In case of a glass substrate (for vacuum tube collectors), also the underlying IR mirror is deposited as a thin film. For flat substrates and interfaces, the optical behavior of the total system can be modeled by the method of the characteristic matrices (see e.g. the description in ref. [35]). However, technical metal sheets exhibit usually a rough surface. This roughness might alter the hemispherical reflectance, but often increases even the optical selectivity. Satisfying absorptance and thermal emittance could be achieved for a-C:H/Cr based multilayered coatings on Cu substrates as can be seen from the step-like bold curve representing the hemispherical reflectivity in fig. 6.

Accelerated aging tests serve to check the durability of these coatings. As aging mechanisms have been identified: oxidation (revealed by XPS), copper diffusion, adhesion failure (both observed by electron microscopy), and graphitization of the a-C:H matrix (revealed by measurements of the Raman effect). The methodology of accelerated aging is described in ref. [36]. A performance criterion determines the service lifetime of the solar absorber. It is defined as

$$PC = -\Delta\alpha + 0.25\Delta\varepsilon \leq 5\% \qquad (3)$$

Based on the assumption of an Arrhenius law, lifetimes t_1, t_2, at different temperatures T_1, T_2, can be interrelated:

$$t_2 = t_1 \cdot \exp[(1/T_2 - 1/T_1)E_a/R] \qquad (4)$$

where E_a is the activation energy of the dominating aging mechanism and R the universal gas constant. The activation energy E_a can thus be found by aging at different elevated temperatures, and a service lifetime prediction can be made for the assumed operating temperature.

The durability of a-C:H/Cr based absorber coatings has been optimized[27]. Hereby, crucial factors have been the appropriate substrate bias voltage during CVD and the choice of a suitable diffusion barrier. Excellent dry heat aging performance could be achieved by employing a diffusion barrier of chromium carbide. Tests under humid conditions have been successful, too. An advantage of amorphous hydrogenated carbon a-C:H is the absence of grain boundaries, which might be susceptible to wet corrosion. For these coatings, a service lifetime of more than 25 years is projected.

The heavy metal chromium could be substituted successfully by the environmentally harmless metal titanium. A satisfying aging stability could be achieved for a-C:H/Ti based coatings on Al substrates[28]. After prolonged tempering, however, a degradation of the optical performance has been detected, most presumably due to the graphitization of the a-C:H matrix and to the oxidation of a-C:H and TiC clusters. The incorporation of silicon into these films results in an enormous enhancement of the heat aging performance[37]. In a comparative experiment, these a–C:H/Ti films showed no measurable degradation, while a-C:H/Ti degraded continuously. Figure 8 shows the evolution of the solar absorption of a-C:H/Ti and a-Si:C:H/Ti based coatings during tempering at 250°C. This effect might be explained by self-passivation (formation of a SiO_2 protective layer), and stabilization against graphitization.

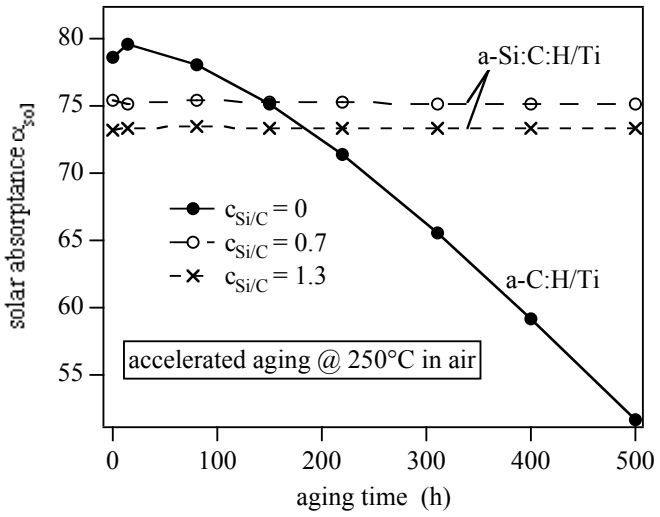

Figure 8: Accelerated aging test of single layered solar absorber coatings at 250°C in air. Displayed is the evolution of the solar absorptance α_{sol} for two series of coatings on aluminum substrates (with and without Ti precoating). The solar absorptance α_{sol} of the a-C:H/Ti coatings drops down significantly, while α_{sol} of the a-Si:C:H/Ti coatings remains constant.

Recently, the commercialization of the developed thin film systems has been initiated by the introduction of a-C:H/Cr based selective solar absorber coatings into the market (IKARUS COATINGS, Germany). The upscaling of the plasma deposition process in the laboratory to the industrial production has been a non-trivial task[38]. The vacuum installation for the industrial production (VON ARDENNE, Germany) is depicted in fig. 9. A roll to roll process allows the coating deposition onto copper bands of 1 m width.

CONCLUSIONS

Manifold research activities have been focusing on the application of nanostructured materials in the field of solar energy conversion. Special physical effects related to the nanometer size scale give rise to interesting macroscopic properties. Examples are nanocrystalline oxides in dye sensitized solar cells, and nanocomposite thin films applied as optically selective absorber coatings. These nanocomposite materials, previously often denoted as cermets, have been successfully transferred to industrial production, and some companies are on the market with different products. As discussed above, new phenomena directly related to nanostructured

materials are currently investigated. Since nanotechnology is a field of considerable research activity these days, these and other new findings may become of interest for solar energy technology.

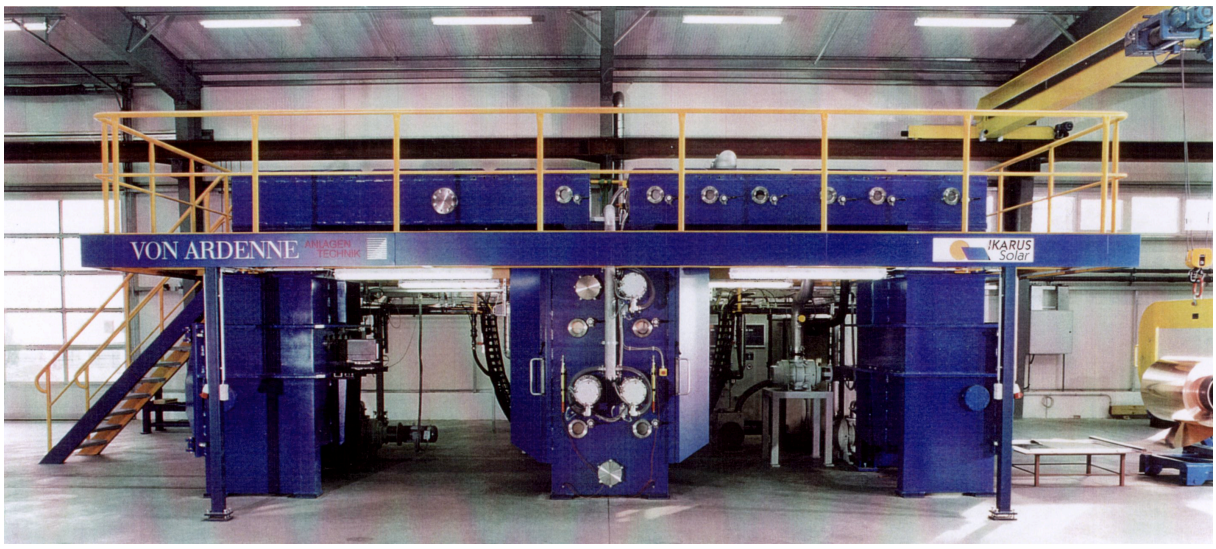

Figure 9: Industrial thin film deposition equipment for selective absorber coatings on copper sheets based on multilayer a-C:H/Cr nanocomposites. The production capacity is in the order of $2 \cdot 10^5$ m^2/year (IKARUS COATINGS, FRG).

ACKNOWLEDGEMENTS

Financial support of the Swiss Federal Office of Energy, the National Center of Competence in Research (NCCR) 'Nanoscale Science' and the Swiss National Foundation SNF is gratefully acknowledged.

REFERENCES

1. Schmid, G., R. Pfeil, R. Boese, F. Bandermann, S. Meyer, G.H.M. Calis, and J.W.A. van der Velden, Chem. Ber., 1981. **114**: p. 3634.
2. Boyen, H.G., G. Kästle, F. Weigl, P. Ziemann, G. Schmid, M.G. Garnier, and P. Oelhafen, Physical-Review-Letters, 2001. **87**: p. 276401/1.
3. Boyen, H.G., G. Kästle, F. Weigl, B. Koslowski, C. Dietrich, P. Ziemann, J.P. Spatz, S. Riethmüller, C. Hartmann, M. Möller, G. Schmid, M.G. Garnier, and P. Oelhafen, Science, 2002. **297**: p. 1533.
4. Gampp, R., *Deposition und Charakterisierung von metallhaltigen, amorphen Kohlenwasserstoffilmen zur Anwendung in Sonnenkollektoren*. Fortschritt-Berichte VDI Reihe 5. Vol. Nr. 446. 1996, Düsseldorf: VDI Verlag GmbH.
5. Gampp, R., P. Gantenbein, and P. Oelhafen in *Film synthesis and growth using energetic beams*. 1995. San Francisco: Materials Research Society.
6. Schüler, A. and P. Oelhafen, Appl. Phys. A, 2001. **73**: p. 237.
7. Schüler, A., *Nanocomposite and nanocrystalline thin films for thermal solar energy applications - deposition and physical characterization*. PhD Thesis, 2000, University of Basel, Switzerland.
8. Niklasson, G.A. and C.G. Granqvist, J. Appl. Phys., 1984. **55**: p. 3382.
9. Jörger, R., R. Gampp, A. Heinzel, W. Graf, M. Köhl, P. Gantenbein, and P. Oelhafen, Solar Energy Materials & Solar Cells, 1998. **54**: p. 351.
10. Smith, G.B., C.A. Deller, P.D. Swift, A. Gentle, P.D. Garrett, and W.K. Fisher, Journal of Nanoparticle Research, 2002. **4**(1-2): p. 157.
11. Grätzel, M., Nature, 2001. **414**: p. 338.

12. Hagfeldt, A., L. Walder, and M. Grätzel, Proceedings of the SPIE The International Society for Optical Engineering, 1995: p. 2531 60.
13. Bencic, S., B. Orel, A. Surca, and U. Lavrencic-Stangar, Solar Energy, 2000: p. 68(6) 499.
14. Kumara, G.R.R.A., F.M. Sultanbawa, V.P.S. Perera, I.R.M. Kottegoda, and K. Tennakone, Solar Energy Materials and Solar Cells, 1999: p. 58(2) 167.
15. Oelerich, W., T. Klassen, and R. Bormann. MRS Symposium 2001 *Synthesis, Functional Properties and Applications of Nanostructures*. San Francisco, CA, USA. 2002.
16. Reim, M., A. Beck, W. Korner, R. Petricevic, M. Glora, M. Weth, T. Schliermann, J. Fricke, C. Schmidt, and F.J. Potter, Solar Energy, 2002. **72**(1): p. 21.
17. Benz, N., T. Beikircher, and B. Aghazadeh, Solar Energy, 1996: **58**(1-3): p. 45.
18. Nostell, P., A. Roos, and B. Karlsson, Thin Solid Films, 1999: **351**(1-2): p. 170.
19. Schelm, S. and G.B. Smith, Applied Physics Letters, 2003. **82**(24): p. 4346.
20. Oles, M., E. Nun, G. Dambacher, and B. Schleich in *1st Annual International IEEE-EMBS Special Topic Conference on Microtechnologies in Medicine and Biology. Proceedings. 12-14 Oct. 2000 Lyon, France*, 2000.
21. Blossey, R., Nature Materials, 2003. **2**(May 2003): p. 301.
22. Geng, J., *Spectral selective coatings based on aluminium oxide and related materials.* 2000, PhD Thesis, University of Basel, Switzerland.
23. Agnihotri, O.P. and B.K. Gupta, *Solar selective surfaces.* 1981: Wiley, New York.
24. Tabor, H. U.S. Patent 2,917,817 (1955).
25. Lazarov, M., P. Raths, H. Metzger, and W. Spirkl, J. of App. Phys., 1995. **77**: p. 2133.
26. Graf, W., F. Brucker, M. Köhl, T. Troscher, V. Wittwer, and L. Herlitze, J. of Non-crystalline Solids, 1997. **218**: p. 380.
27. Gampp, R., P. Oelhafen, P. Gantenbein, S. Brunold, and U. Frei, Solar Energy Materials & Solar Cells, 1998. **54**: p. 369.
28. Schüler, A., J. Geng, P. Oelhafen, S. Brunold, P. Gantenbein, and U. Frei, Solar Energy Materials and Solar Cells, 2000. **60**: p. 295.
29. Schüler, A., R. Gampp, and P. Oelhafen, Phys. Rev. B, 1999. **60**: p. 16164.
30. Maxwell-Garnett, J.C., Philos. Trans. R. Soc. London, Ser. A, 1904. **203**: p. 385.
31. Maxwell-Garnett, J.C., Philos. Trans. R. Soc. London, Ser. A, 1906. **205**: p. 237.
32. Bruggeman, D.A.G., Ann. Phys. 5. Folge, 1935. **24**: p. 636.
33. Sheng, P., Phys. Rev. Lett., 1980. **45**: p. 60.
34. Schüler, A., C. Ellenberger, P. Oelhafen, C. Haug, and R. Brenn, J. Appl. Phys., 2000. **87**(9): p. 4285.
35. Macleod, H.A., *Thin-Film Optical Filters.* 1986, 2001, Bristol and Philadelphia: Institute of Physics Publishing.
36. Frei, U. et al. in Optical materials technology for energy efficiency and solar energy conversion XIV, Proc. SPIE 2531, 1995, p.282.
37. Schüler, A., I.R. Videnovic, P. Oelhafen, and S. Brunold, Solar-Energy-Materials-and-Solar-Cells, 2001. **69**: p. 271.
38. Milde, F., M. Dimer, C. Hecht, D. Schulze, and P. Gantenbein, Vacuum, 2000. **59**(2-3): p. 825.